chemosensors

Article

Aminoquinoxaline-Based Dual Colorimetric and Fluorescent Sensors for pH Measurement in Aqueous Media

Elizaveta V. Ermakova [1,*], Andrey V. Cheprakov [2] and Alla Bessmertnykh-Lemeune [3,4,*]

[1] Frumkin Institute of Physical Chemistry and Electrochemistry, Russian Academy of Sciences, Leninsky Pr. 31-4, Moscow 119071, Russia
[2] Department of Chemistry, Lomonosov Moscow State University, 1-3, Leninskie Gory, Moscow 119991, Russia
[3] Institut de Chimie Moléculaire de l'Université de Bourgogne, CNRS UMR 6302, Université Bourgogne Franche-Comté, 9 Avenue Alain Savary, BP 47870, 21078 Dijon, France
[4] Laboratoire de Chimie, CNRS UMR 5182, ENS de Lyon, 46 Allée d'Italie, 69364 Lyon, France
* Correspondence: dr.evermakova@phyche.ac.ru (E.V.E.); alla.lemeune@ens-lyon.fr (A.B.-L.)

Abstract: This research is focused on the development of pH indicators based on the quinoxaline signaling group for acidic aqueous solutions (pH 1–5). A push–pull quinoxaline **QC1** in which two electron-donating (3-aminopropyl)amino substituents are attached to positions 6 and 7 of the electron-deficient quinoxaline moiety was prepared using the palladium-catalyzed C–N cross-coupling reaction. The 3-aminopropyl residues are mostly protonated in aqueous solutions below pH 8, thus serving as hydrophilizing substituents that render quinoxaline derivative **QC1** water-soluble in this range of acidities and useful for measurements in the pH range of 1–5. This chromophore is a dual optical chemosensor that exhibits shifts of both absorption and emission bands in response to external stimuli. The presence of naturally relevant metal cations (13 ions) does not interfere with spectrophotometric and fluorescence measurements of the optical response of aminoquinoxaline in the visible region. Moreover, these spectral changes are easily observed by the naked eye, allowing for rapid semi-quantitative analyses under "in-field" conditions.

Keywords: quinoxaline; pH indicator; colorimetry; fluorescence; optical chemosensor

Citation: Ermakova, E.V.; Cheprakov, A.V.; Bessmertnykh-Lemeune, A. Aminoquinoxaline-Based Dual Colorimetric and Fluorescent Sensors for pH Measurement in Aqueous Media. *Chemosensors* **2022**, *10*, 342. https://doi.org/10.3390/chemosensors10080342

Academic Editor: Jun Wang

Received: 28 July 2022
Accepted: 19 August 2022
Published: 21 August 2022

1. Introduction

Quinoxalines are widely investigated due to their useful optical properties and the possibility of their functionalization by both electron-donating and electron-withdrawing substituents and incorporation into macrocycles, push–pull molecules and polymer chains required for many specific applications [1–11]. In particular, these photoactive and biocompatible compounds are widely used for labeling, sensing and imaging [12]. They have been employed as chemosensors for anions [13], cations [14], small molecules [15–18] and biologically relevant targets [19–21].

These compounds are also widely used to measure the acidity of solutions. Rapid and real-time monitoring of this simple parameter is ubiquitously used in industry and environmental monitoring [22–24]. Therefore, pH indicators suitable for a wide range of experimental conditions are still required. The ability of quinoxalines to change optical properties upon protonation of the heterocycle has been thoroughly investigated to prepare colorimetric and fluorescent proton-sensitive indicators for gaseous [25,26] and liquid samples [16,18,26–36]. Due to their low basicity, these compounds change color in media with relatively high acidity (pH < 4), in which most known pH chemosensors are insensitive [37–41]. This pH region is relevant to many clinical and environmental analyses because it sometimes even occurs in living organisms (in the human stomach, for instance) and should be controlled in many industrial processes (monitoring of wastes and groundwater in the production of lead–acid batteries), which might contribute to leakage of highly acidic water to the environment [23,42,43]. However, most of the quinoxaline derivatives reported so far

for monitoring acidity can be used only in organic solvents or binary solvent mixtures due to their low solubility in aqueous media and are still inconvenient for real-world analyses, which commonly need to be performed in media free of organic co-solvents.

In this work, we prepared a new push–pull quinoxaline **QC1** in which the acceptor quinoxaline moiety is functionalized by hydrophilic electron-donating (3-aminopropyl)amino substituents (Figure 1) and investigated its halochromic properties.

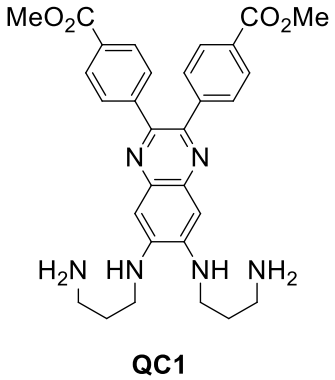

QC1

Figure 1. Structure of aminoquinoxaline **QC1** investigated in this work.

We demonstrated that the optical chemosensor **QC1** allows for dual-channel pH monitoring in aqueous samples at a pH range of 1–5 due to red shifts of absorption and emission bands after protonation of the heteroaromatic ring. This indicator exhibits optical responses in the visible region and can be used for semi-quantitative naked-eye pH estimates. To our knowledge, this is the first example of pH indicators with a quinoxaline signaling group that can be used for the analysis of aqueous samples without the addition of any organic co-solvents.

2. Materials and Methods

2.1. General Considerations

Unless otherwise noted, all chemicals and starting materials were obtained commercially from Acros (via Fisher Scientific, Illkirch, France) or Sigma-Aldrich (via Merck Co., St. Quentin Fallavier, France) and used without further purification. 4,4′-Bis(methoxycarbonyl) benzil (**1**) was prepared according to published procedures [44]. Cs_2CO_3 was dried under reduced pressure at 120 °C for 48 h. Chloroform (analytical grade) for physicochemical studies was purchased from Merck (St. Quentin Fallavier, France).

All metal salts used were perchlorates of the general $M(ClO_4)n{\cdot}x\ H_2O$ formula. ***Caution:*** Although no problems were experienced, perchlorate salts are potentially explosive when combined with organic ligands and should be manipulated with care and used only in very small quantities.

^1H and ^{13}C spectra were acquired either on a Bruker Avance III Nanobay 300 MHz or a Bruker Avance III 500 MHz spectrometer (Bruker France, Wissembourg, France). Chemical shifts are expressed in parts per million (ppm), referenced on the δ scale by using residual non-deuterated solvent signals as an internal standard for ^1H and ^{13}C NMR spectroscopy. The coupling constants are expressed in units of frequency (Hz). Accurate mass measurements (HRMS) were made on a THERMO LTQ Orbitrap XL (Thermo Fisher Scientific, Asnières-sur-Seine, France) equipped with an electrospray ionization (ESI) source in positive mode unless otherwise stated. Solutions in $CHCl_3$/methanol (1:1 v/v) were used for the analysis. IR spectra were registered on a Bruker Vector 22 spectrophotometer (Bruker, Wissembourg, France). A universal micro-ATR sampling accessory (Pike Technologies, Fitchburg, MA, USA) was used in order to obtain IR spectra of solid samples. MALDI-TOF mass spectra were obtained on a Bruker Ultraflex II LRF 2000 mass spectrometer (Bruker, Wissembourg, France) in positive ion mode with dithranol matrix. Analytical thin-layer

chromatography (TLC) was carried out using Merck (St. Quentin Fallavier, France) silica gel 60 F-254 plates (precoated sheets, 0.2 mm thick, with fluorescence indicator F254).

All spectrometers were available at "Pôle Chimie Moléculaire", the technological platform for chemical analysis and molecular synthesis (http://www.wpcm.fr, accessed on 20 June 2022), which relies on the Institute of the Molecular Chemistry of University of Burgundy and WelienceTM, a Burgundy University private subsidiary.

2.2. Synthesis of Aminoquinoxalines

2,3-Bis(4-methoxycarbonylphenyl)-6,7-dibromoquinoxaline (3). A 50 mL two-necked flask equipped with a magnetic stirrer and a back-flow condenser was charged with 4,4′-bis(methyloxycarbonyl)benzil (**1**) (164 mg, 0.5 mmol) in 50 mL of acetic acid. Subsequently, 4,5-dibromo-1,2-benzenediamine (**2**) (160 mg, 0.6 mmol) was added, and the mixture was stirred at reflux for 24 h. After that, the reaction mixture was cooled to room temperature and stirred for 8 h. The suspension was filtered and dried in vacuo. The target compound (**3**) was isolated as an orange-brown solid in 89% yield (247 mg). ^{1}H NMR (500 MHz, DMSO-d_6, 25 °C): δ_H = 3.88 (s, 6H, OCH_3), 7.62 (d, J = 8.4 Hz, 4H, H_{Ar}), 7.94 (d, J = 8.4 Hz, 4H, H_{Ar}) and 8.61 (s, 2H, H_Q) ppm. ^{13}C NMR (500 MHz, DMSO-d_6, 25 °C): δ_C = 52.61 (2C, OCH_3), 126.78 (2C, C_{Br}), 129.37 (4C, CH_{Ar}), 130.55 (4C, CH_{Ar}), 130.82 (2C, C_{Ar}), 133.53 (2C, CH_Q), 140.54 (2C, C_N or C_{Ar}), 142.79 (2C, C_N or C_{Ar}), 153.92 (2C, C_N) and 166.23 (2C, $\underline{C}O_2CH_3$) ppm. IR (neat): υ_{max} (cm^{-1}) 3394 (w), 3360 (w), 3339 (w), 3315 (w), 3258 (w), 3081 (w), 2996 (w), 2948 (w), 2903 (w), 2843 (w), 2659 (w), 2360 (w), 2341 (w), 2165 (w), 2148 (w), 2108 (w), 2077 (w), 1981 (w), 1931 (w), 1811 (w), 1718 (s), 1609 (m), 1583 (m), 1572 (m), 1533 (w), 1509 (w), 1436 (m), 1412 (m), 1399 (m), 1336 (m), 1313 (m), 1277 (s), 1188 (m), 1104 (s), 1055 (m), 1018 (m), 980 (m), 964 (m), 931 (m), 898 (m), 859 (m), 828 (m), 770 (m), 730 (m), 722 (m), 706 (s), 693 (m), 647 (m), 639 (m), 616 (m), 605 (m), 551 (m), 517 (m) and 511 (m). HRMS (ESI): m/z calcd. for $C_{24}H_{17}Br_2N_2O_4$ $[M + H]^+$ 554.95496, found 554.95470; calcd. for $C_{24}H_{16}Br_2N_2NaO_4$ $[M + Na]^+$ 576.93,690, found 576.93,612.

2,3-Bis(4-methoxycarbonylphenyl)-6,7-bis[(3-aminopropyl)amino]quinoxaline (QC1). A 250 mL two-necked flask equipped with a magnetic stirrer and a back-flow condenser was charged with 2,3-bis(4-methoxycarbonylphenyl)-6,7-dibromoquinoxaline (**3**) (2.0 g, 3.597 mmol), dppf (320 mg, 0.576 mmol), $Pd(dba)_2$ (166 mg, 0.288 mmol) and sodium *tert*-butoxide (518 mg, 5.396 mmol). The reaction vessel was evacuated and purged with N_2 three times. Subsequently, 60 mL of dioxane was added with a syringe, and the mixture was stirred. After that, 1,3-diaminopropane (1.8 mL, 21.582 mmol) was added with a syringe, and the mixture was stirred at reflux for 48 h. Then, the reaction mixture was cooled to room temperature, diluted with CH_2Cl_2 (200 mL), washed with water (2 × 50 mL), dried over $MgSO_4$ and evaporated under reduced pressure. The residue was purified by column chromatography on silica gel using CH_2Cl_2, CH_2Cl_2/MeOH (80:20 v/v), CH_2Cl_2/MeOH (60:40 v/v) and CH_2Cl_2/MeOH/Et_3N (60:40:20 $v/v/v$) as eluents. The target compound (**QC1**) was isolated as a yellow-orange solid in 25% yield (488 mg). ^{1}H NMR (300 MHz, CD_3OD, 25 °C): δ_H = 2.16 (br t, 4H, $NHCH_2C\underline{H}_2CH_2NH_2$), 3.12 (br t, 4H, $C\underline{H}_2NH_2$), 3.40 (br t, 4H, $NHC\underline{H}_2$), 3.84 (br s, 6H, OCH_3), 6.83 (s, 2H, H_Q), 7.39 (d, J = 8.2 Hz, 4H, H_{Ar}) and 7.87 (d, J = 8.2 Hz, 4H, H_{Ar}) ppm. NH and NH_2 protons were not unambiguously assigned. ^{13}C NMR (300 MHz, CD_3OD, 25°C): δ_C = 25.59 (2C, $NHCH_2\underline{C}H_2CH_2NH_2$), 37.97 (2C, CH_2NH_2), 40.50 (2C, $NHCH_2$), 52.17 (2C, OCH_3), 101.42 (2C, CNH), 129.40 (4C, CH_{Ar}), 129.63 (2C, CH_Q), 129.93 (4C, CH_{Ar}), 138.67 (2C, C_{Ar}), 142.20 (2C, C_N or C_{Ar}), 143.96 (2C, C_N or C_{Ar}), 146.51 (2C, C_N) and 167.17 (2C, $\underline{C}O_2CH_3$) ppm. IR (neat): υ_{max} (cm^{-1}) 3381 (w), 3370 (w), 3355 (w), 3327 (w), 3315 (w), 3277 (w), 3261 (w), 3243 (w), 3231 (w), 3219 (w), 3195 (w), 3178 (w), 3157 (w), 3132 (w), 3115 (w), 3060 (w), 3040 (w), 2988 (w), 2961 (w), 2925 (w), 2852 (w), 2812 (w), 2652 (w), 2632 (w), 2531 (w), 2449 (w), 2349 (w), 2324 (w), 2288 (w), 2236 (w), 2221 (w), 2190 (w), 2165 (w), 2144 (w), 2107 (w), 2088 (w), 2064 (w), 2050 (w), 2015 (w), 1981 (w), 1961 (w), 1903 (w), 1842 (w), 1722 (w), 1606 (w), 1505 (w), 1464 (w), 1436 (w), 1404 (w), 1359 (w), 1278 (w), 1211 (w), 1178 (w), 1104 (w),

1019 (w), 982 (w), 865 (w), 781 (m), 631 (m), 536 (m) and 505 (s). HRMS (ESI): m/z calcd. for $C_{30}H_{35}N_6O_4$ $[M + H]^+$ 542.27143, found 543.27073.

2.3. UV–vis Absorption and Fluorescence Measurements

UV–vis absorption spectra were recorded on a SHIMADZU-2450 spectrometer (Shimadzu, Kyoto, Japan) in a wavelength range of 200–800 nm. The fluorescence spectra were recorded on a SHIMADZU RF-5301 spectrofluorometer (Shimadzu, Kyoto, Japan) in a wavelength range of 200–800 nm. The measurements were performed in a quartz cuvette with an optical path length of 1 cm at 25 ± 1 °C.

Fluorescence quantum yields were measured at 25 °C by a relative method using fluorescein in ethanol (Φ = 92%) as a standard [45]. The following equation was used to determine the relative fluorescence quantum yield:

$$\Phi_x = \Phi_{st} ((F_x \cdot A_{st} \cdot \eta_x{}^2)/(F_{st} \cdot A_x \cdot \eta_{st}{}^2)), \quad (1)$$

where A is the absorbance (in the range of 0.01–0.1), F is the area under the emission curve, η is the refractive index of the solvents (at 25 °C) used for the measurements, and the subscripts x and st represent the sample under study and standard compound. The following refractive index values were used: 1.333 for water, 1.362 for ethanol and 1.445 for chloroform.

2.4. Determination of Protonation Constants

pH measurements were carried out using a portative Ecotest 2000 pH meter (Econix, Moscow, Russia) with a combined ESK-10601/7 glass electrode. The electrode was calibrated with commercial buffers (pH = 4.01, 6.86 and 9.18). Protonation studies were conducted in a glass beaker equipped with a magnetic stirrer and pH electrode. Aliquots of acid (1M HCl) or base (1M KOH) were added manually with a Hamilton microsyringe to **QC1** aqueous solution (0.112 mM for spectrophotometric and 0.015 mM for fluorescence titrations, respectively) containing potassium chloride (0.1 M). The measurements were performed in a quartz cuvette with an optical path length of 1 cm at 25 ± 1 °C. The excitation wavelength of aminoquinoxaline **QC1** was 420 nm. The entire multiwavelength data sets were decomposed into their principal components by factor analysis before adjusting the equilibrium constants and extinction coefficients by nonlinear least-squares analysis with the HypSpec program [46].

*2.5. NMR Studies of Protonation of **QC1***

Solutions of D_2O with different pH values (1.0, 2.0, 3.0, 4.0, 5,0, 6.0, 7.0, 8.0 and 9.0) were prepared by adding deuterium chloride solution in D_2O or sodium deuteroxide in D_2O to 1 mL of D_2O. pH measurements were carried out using a portative Ecotest 2000 pH meter (Econix, Moscow, Russia) with a combined ESK-10601/7 glass electrode. The electrode was calibrated with commercial buffers (pH = 4.01, 6.86 and 9.18). The pD values of these solutions can be obtained from a calibrated pH electrode by adding a correction constant of about 0.4 if required. Then, a 1mM solution of **QC1** was prepared by dissolving a sample of the compound in each of the prepared solutions. The studied samples were placed in an NMR tube and investigated using a Bruker Avance 400 MHz spectrometer (Bruker, Wissembourg, France) at room temperature.

^1H spectra were acquired for the nine samples, and selected data are presented in Supplementary Materials. Chemical shifts are expressed in parts per million (ppm), referenced on the δ scale by using residual non-deuterated solvent signals as an internal standard, and the pH scale was used for qualitative interpretation of data thus obtained.

2.6. DFT Calculations

The structure of **QC1** was modeled by DFT calculations using the Firefly quantum chemistry package [47], which is partially based on the GAMESS (US) [48] source code. The calculations were performed using the B3LYP functional with the STO 6-31G(d,p) basis

set for all elements; at each step, full optimization of geometry was achieved, and the minima were confirmed by computing vibration frequencies. The modeling was performed by replacing aryl substituents with phenyl groups and 3-aminopropyl substituents at the nitrogen atoms with smaller methyl groups. This compound was labeled **QC-Me**, and its protonated forms were labeled **QC-MeH$_{Ar}$** and **QC-MeH$_{Q}$** for species in which aromatic and heterocyclic nitrogen atoms are protonated, respectively.

3. Results

*3.1. Synthesis of Aminoquinoxaline **QC1***

Aminoquinoxaline **QC1** was synthesized according to the reaction sequence shown in Scheme 1.

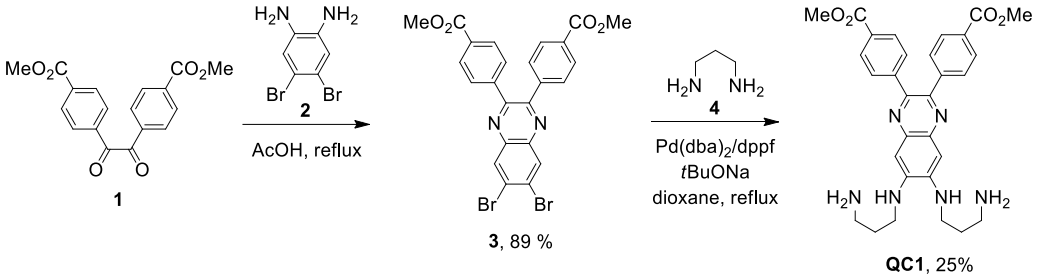

Scheme 1. Synthesis of aminoquinoxaline **QC1**.

First, 4,4′-bis(methoxycarbonyl)benzil (**1**) was prepared from commercially available methyl 4-formylbenzoate as described by Krebs et al. [44]. This compound was reacted with 4,5-dibromo-1,2-benzenediamine (**2**) in acetic acid at reflux to obtain dibromoquinoxaline **3** in 89% yield. 5-Arylamino-substituted quinoxalines can be prepared by using the palladium-catalyzed C–N cross-coupling reaction [49–52]. This reaction was also successfully used for the preparation of chemosensors [53–59] because linear polyamines bearing diaminoethane or diaminopropane residues can be mono-arylated without employing laborious protection–deprotection steps [60]. However, the substitution of both adjacent bromine atoms in the aromatic ring is usually a challenging task [61].

Our preliminary experiments on the amination of 6,7-dibromoquinoxaline **3** by 1,3-diaminopropane under standard conditions of the Buchwald–Hartwig reaction [62] (Pd(dba)$_2$/BINAP, sodium *tert*-butylate (*t*BuONa) and 1,4-dioxane at reflux) were unsuccessful (Table 1, entry 1). The same result was obtained with DavePhos ligand (entry 2) and cesium carbonate as a base (entry 3). In the presence of dppf ligand, the reaction took place, but with a low selectivity. The substitution of the second bromine atom was still incomplete after 24 h of reflux, and mono- and diaminated products were obtained in about a 1:1 ratio. Their chromatographic separation gave the target diamine in 21% yield. When the reaction time was increased to 72 h, diaminoquinoxaline **QC1** was isolated in low 12% yield, probably due to its partial decomposition during prolonged heating in the presence of a strong base (entry 5). A slight increase in yield was obtained when increasing the reaction time from 24 h to 48 h (entry 6).

The newly synthesized compounds **1**, **3** and **QC1** were unambiguously characterized by NMR, IR, UV–vis and HRMS (ESI) analyses.

It is worth noting that, in this compound, electron-donating amino residues are attached to positions 6 and 7 of the heterocycle, while in most push–pull quinoxaline derivatives reported elsewhere in the literature, the donor substituents are present in positions 2 and 3 of the electron-deficient heteroaromatic system [32,63,64]. Derivatives bearing donor moieties in positions 6 and 7 are scarcely studied; for instance, 6-amino-2,3-diphenylquinoxaline (**QArN**) [65] and quinoxalines with fused electron-rich tetrathiafulvalene subunits were investigated [35].

Table 1. Palladium-catalyzed amination of 6,7-dibromoquinoxaline **3** with 1,3-diaminopropane [1].

Entry	L	t, h	Conversion, % [2]	Yield of QC1, % [2]
1	BINAP [3]	72	0	0
2	DavePhos [4]	72	0	0
3 [5]	BINAP	72	0	0
4	dppf [6]	24	100	21 [7,8]
5	dppf	72	100	12 [8]
6	dppf	48	100	25 [8]

[1] Reaction conditions: bromide **3** (0.5 mmol), 1,3-diaminopropane (6 equiv.), $Pd(dba)_2$/L (0.08/0.16 equiv.) and sodium *tert*-butoxide (1.5 equiv.) in 1,4-dioxane at reflux under N_2. The reaction course was monitored by MALDI-TOF spectrometry. [2] Determined by ^{1}H NMR analysis. [3] BINAP = 2,2′-bis(diphenylphosphino)-1,1′-binaphthyl. [4] DavePhos = 2-dicyclohexylphosphino-2′-(*N*,*N*-dimethylamino)biphenyl. [5] Cs_2CO_3 was employed as a base. [6] dppf = 1,1′-ferrocenediyl-bis(diphenylphosphine). [7] Mixture of mono- and diamines according to NMR analysis. [8] Isolated yield of diamine **QC1**.

*3.2. Photophysical Studies of Quinoxaline **QC1** in Chloroform Solution*

The electronic absorption and emission spectra of **QC1** in chloroform are presented in Figure S1, and the data are summarized in Table 2, which also includes the parameters for the reference compounds, 2,3-dimethylquinaxoline (**QMe**), 2,3-di[4-(*N*-phenyl-*N*-naphthylamino) phenyl]quinoxaline (**QAr**) and 6-amino-2,3-diphenylquinoxaline (**QArN**). Aminoquinoxaline **QC1** exhibits absorption bands typical for quinoxaline derivatives [12,65]. The intense absorption bands in the 250–350 nm region can be assigned to $\pi-\pi^*$ electronic transitions, while the absorption in the visible region (400–500 nm) is propably due to charge transfer transitions **[66].** Notably, the replacement of methyl substituents in quinoxaline **QMe** by aryl groups (**QAr** and **QArN**) or diaminopropane residues (**QC1**) results in a large red shift of the absorption band in the visible region, probably due to enhanced electronic coupling of electron-rich substituents with the electron-deficient aromatic core. Remarkably, high molar absorptivity in the visible region is important for the application of compound **QC1** as an optical sensor.

Table 2. Photophysical data for aminoquinoxaline **QC1** and the reference compounds in chloroform solution.

Ligand	λ_{abs}, nm (log (ε, cm^{-1} M^{-1}))	λ_{em}, nm [1]	Φ_{em} [2]	Reference
QC1	308 (3.76), 420 (3.69)	472	0.244	this work
QMe [3]	237 (4.39), 315 (3.84)			[65]
QAr [4]	305 (4.23), 399 (4.33)	530	0.170	[66]
QArN [3]	245 (4.37), 265 (4.35) 292(4.41), 407(4.00)			[65]

[1] Emission was excited at 420 nm. [2] Measured in chloroform at ambient temperatures relative to a solution of fluorescein in ethanol as a standard. [3] In 95% ethanol solution. [4] In dichloromethane solution. See text for names of **QMe**, **QAr** and **QArN**.

Aminoquinoxaline **QC1** is brightly emissive in chloroform at room temperature, and emissive bands appear in the region of 430–580 nm. The attachment of two (3-aminopropyl)amino moieties to the quinoxaline ring does not enhance the non-radiative quenching of the fluorescence, and the emission quantum yield value (Φ_{em}) of **QC1** is close to that of **QAr**.

*3.3. Protonation Studies of Aminoquinoxaline **QC1** in Aqueous Media*

Compound **QC1** is soluble in water, probably due to spontaneous protonation of the relatively highly basic aliphatic amino groups. In acidic solutions, it can be further protonated, which results in a substantial change in photophysical properties, and we studied these phenomena by UV–vis and fluorescence spectroscopies. Both the absorption and emission parameters of the compound under study progressively changed upon the

gradual addition of hydrochloric acid in 11.5–6.5 and then 5.0–1.0 pH ranges, as shown in Figures 2 and S2.

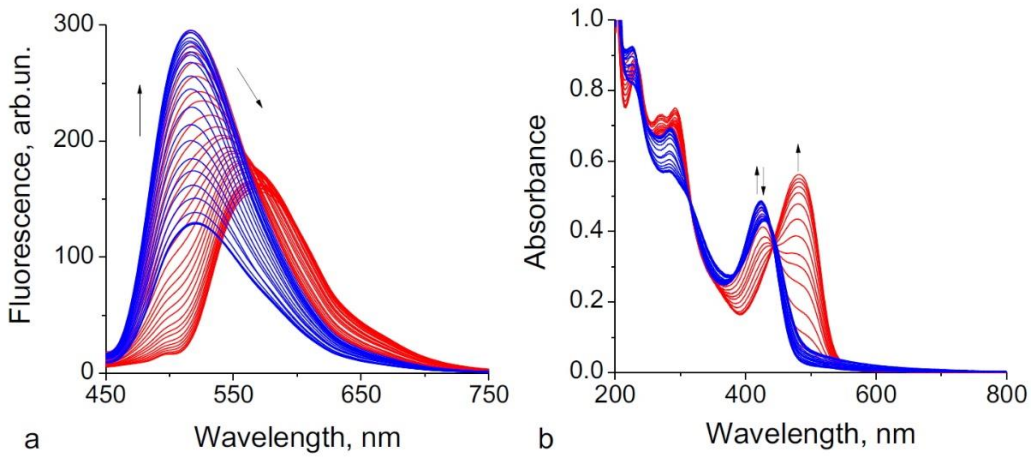

Figure 2. Fluorescence (**a**) and spectrophotometric (**b**) titration of **QC1** in an aqueous solution as a function of pH. (**a**) $[\mathbf{QC1}]_{tot}$ = 0.015 mM, pH = 11.49–1.00 (11.49–6.11 (blue), 5.92–1.00 (red)); λ_{ex} = 420 nm, I = 0.1 M KCl. (**b**) $[\mathbf{QC1}]_{tot}$ = 0.112 mM, pH = 11.53–1.01 (11.53–6.04 (blue), 5.89–1.01 (red)); I = 0.1 M KCl. The arrows demonstrate trends of emission and absorption intensity changes with pH.

In the visible-region fluorescence spectra exhibit a broad emission band of low intensity under basic conditions (Figure 2a). When pH decreases from 11.5 to 6.1, this band is red-shifted by only 8 nm, and this shift is accompanied by an increase in band intensity (Φ_{em} = 0.021–0.048, Table S1). Such variations in emission are commonly observed in amino-substituted chromophores upon protonation of the side-chain amine group, presumably as a result of suppression of the PET process upon protonation of the amine donor group electronically decoupled from the emissive fragment. Further acidification of the solution towards pH = 1.0 leads to a much stronger red shift of the emission band maxima to 570 nm and a small increase in emission quantum yield (Φ_{em} = 0.048–0.061, Table S1). This change in the emission band is most likely associated with further protonation of the fluorophore.

It is worth noting that quinoxaline-based optical chemosensors in which pH changes lead to a shift of the emission maximum are scarce, and in most of them, the quinoxaline system is incorporated in a larger conjugated system [18,25,27,32,36].

The absorption spectra are also sensitive to pH variation (Figure 2b). The stepwise addition of hydrochloric acid to an aqueous solution of **QC1** from pH = 11.5 to pH = 6.0 results in a continuous blue shift of the band maximum from λ_{max} = 430 to 420 nm. Similar to what is observed in the fluorescence spectra, further acidification leads to a much larger change: the absorbance maximum is red-shifted to 480 nm. The spectral changes accompanying the acidification can be monitored visually by comparison of the solution color in daylight (light absorption) and under irradiation by a blue LED (λ_{ex} = 365 nm) (emission of light), thus allowing for a simple rough estimate of acidity without any instrumentation (Figure 3).

Notably, the aqueous solutions in the 0.027–0.319 mM range perfectly obeyed the Beer–Lambert law at all pH values of interest, as shown in Figure S3, revealing that **QC1** is not subject to aggregation, which could have been expected, as the compound lacks well-known truly effective hydrophilizing residues and relies only on the positive charge of the protonated primary amino groups. Thus, in this range of concentrations, it is safe to use it for quantitative and semi-quantitative pH monitoring in aqueous solutions.

To determine apparent protonation constants, numerical data fitting of fluorescence and spectrophotometric titration curves was performed using the HypSpec program [46]. The best fit for the data recorded between pH 1.0 and 11.5 was obtained when the data were processed with a three-species model ($L–LH^{2+}–LH^{3+}$) and gave pK_{a1} values of 9.32 and

10.25 and pK_{a2} values of 3.07 and 2.61 for fluorescence and spectrophotometric titrations, respectively. Titration curves and distribution diagrams and simulated electronic absorption and fluorescence spectra of **QC1** and their protonated forms calculated with the HypSpec program are shown in Figures 2b and S4–S6.

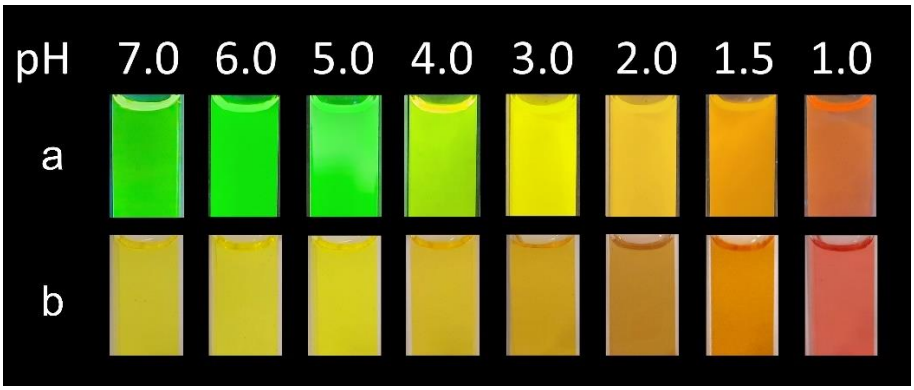

Figure 3. pH-induced color changes of **QC1** (0.5 mM) aqueous solution (**a**) under irradiation by LED (λ_{ex} = 365 nm) and (**b**) in daylight.

The protonation sequence can be proposed based on electronic absorption and emission data and general considerations (Scheme 2a). As compound **QC1** contains two side chains terminated with an aliphatic amino group, the first protonation sites are obvious. The basicity of aliphatic amines is usually in the pK_a 10–12 range, which is in perfect agreement with the first constant measured in this work. As the side chains are independent and distant from each other, the influence of the first protonation on the basicity of the second amine could be negligible, and thus, we may expect to observe full protonation of both amino groups upon dissolution of **QC1** in water in the absence of added alkali. We believe that this explains the good solubility of the compound in water, as the ammonium groups are known to be highly hydrophilic, in our case outweighing all other factors, as all other parts of this molecule are not hydrophilic to any extent. In titrations, we enter the alkaline range of pH, which will inevitably deprotonate the cation and render the compound less hydrophilic and less soluble in water, but this is not important for the projected application, as we suggest it to be used only below pH 7, where the compound is safely diprotonated, highly soluble and not prone to aggregation.

The more challenging task is to assign the second pK_a value, equal to 2.61 (spectrophotometric data), as there is ambiguity of which nitrogen atom, the heteroatom in the ring or aromatic amine, is more basic. As these atoms are involved in conjugation, their properties associated with the lone pairs are correlated through electronic effects. Everybody knows the textbook case of 2- and 4-aminopyridines (2-aminopyridine (**Py**) is shown in Scheme 2b), in which the conjugation drastically decreases the basicity of the amino group and enhances the basicity of pyridine nitrogen, so it is the latter that is unambiguously protonated or accepts the attack of electrophiles. In this case, however, the assignment of the more basic site is unambiguous, as we may argue that the estimates of initial basicity excluding the mesomeric interaction are roughly equal: both the pyridine nitrogen and aromatic nitrogen (in, e.g., aniline) have pK_a close to 5 units. Thus, when we take into account the mesomeric interaction, the basicity of the aromatic amine decreases (this group is a donor site in the conjugation path), and the basicity of heterocyclic nitrogen increases (this atom is the acceptor site in the conjugation path); therefore, their relative basicities diverge in opposite directions and become dramatically different. However, if we try to apply this scheme of reasoning to the molecule under study, we come across ambiguity right at the beginning. The problem is that the basicities of diazines (pyrazine, pyrimidine and pyridazine; 2-aminopyrazine (**Pyraz)** is shown in Figure 2b) are much lower than the basicity of monoazines (**Py**, for instance): the published values of pK_a are around 1–2 units. The amino group in **QC1** is also in the conjugation path, though separated by a benzo ring,

but assembled in such a way that the conjugation is maintained (the methyl-substituted analogue **QC-Me**) is shown in Scheme 2b). Thus, there should not be any substantial difference between the analogous 2-aminopyrazine (**Pyraz**) and 6-aminoquinoxaline (**Quin**), as the latter is a vinylogous system with respect to the former (Scheme 2b).

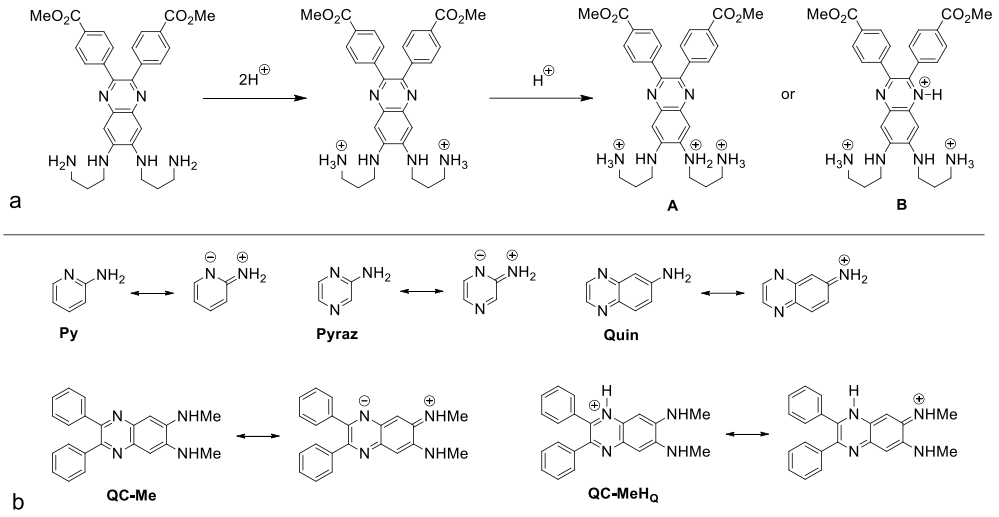

Scheme 2. (**a**) Protonation sequence for quinoxaline **QC1**. (**b**) Structures of amino-substituted aromatic heterocycles **Py**, **Pyraz**, **Quin**, **QC-Me** and **QC-MeH$_Q$**. Triprotonated tautomers of **QC1** are labeled as **A** and **B**.

Therefore, unlike the case of aminopyridines, where the initial estimate diverged upon inclusion of the mesomeric effect, in the case of aminopyrazine **Pyraz** or aminoquinoxaline **Quin**, the estimates would move towards each other by an unknown increment (the basicity of heterocyclic nitrogen would increase from initial pK_a ca. 1, while the basicity of the aromatic amine would decrease from the initial estimate of pK_a ca. 5). Even more confusion would result if we include the second amino group in the scheme: the basicities of aromatic *ortho*-amino groups are known to increase a little due to both lone pair repulsion and hydrogen bonds in the monoprotonated species. Thus, we would only introduce further uncertainty to the estimates.

Therefore, we resorted to DFT computations in an attempt to gain a more definite source of reasoning. To be clear, we did not attempt to achieve a qualitative estimate of basicity constants, as such computations are still quite unreliable but very time-consuming. Instead, we chose to rely on the much simpler computation of the electronic structure of both possible protonated species in the hope that the comparison would reveal a substantial and unambiguous difference that could be related to experimental findings. The model compounds, 2,3-dipehenyl-6,7-bis(*N*-methylamino)quinoxaline (**QC-Me**) and two monoprotonated species **QC-MeH$_{Ar}$** and **QC-MeH$_Q$**, were computed at the DFT B3LYP//STO 6-31G(d,p) level of theory (Figure 4). We argued that the methoxycarbonyl substituent of **QC-1** can be omitted, and the 3-aminopropyl chain can be safely truncated to methyl, as it can be expected to not cause a substantial disturbance in the electronic structure of the model molecules. The geometry of the model compounds was fully optimized, and the assignment to the true minima was ascertained by computing vibrational modes, all of which were positive. The most essential results are presented in Figure 4, where the frontier orbitals are shown at the same scale and formally aligned at the respective HOMO levels.

First of all, we see that in all three model compounds, the frontier orbitals are well separated from the underlying and overlying manifolds; thus, we can safely suppose that the lowest energy transitions and the first excited states can be approximated as HOMO–LUMO interaction without substantial admixture of other MOs. All frontier orbitals in all three models are of a π-nature; thus, the absorption and emission bands in the visible region should be considered as π–π^* transitions. There is a temptation to consider, by

following the obvious analogies with many known organic dyes, the lowest transitions in such molecules to be a charge-transfer transition, and this explanation is often used to explain the appearance of color due to the shift of absorption bands to the visible region, which takes place in molecules involving a conjugation path between a π-donor and a π-acceptor. However, no clear criteria for differentiating the charge-transfer transition from the more common π–π* transition exist; the borderline is wide and blurred. Commonly, in order to meaningfully apply the charge-transfer label to a transition, the frontier orbitals need to be at least partially localized over the donor and acceptor parts of a conjugated system, with both HOMO and LUMO orbitals (orbital sets) being differently delocalized so that a unidirectional shift of electronic density upon transition can be seen. However, this is not the case with the models under study: both HOMO and LUMO are almost uniformly delocalized in a similar manner over the whole π-system. Therefore, the reason why all of the compounds under study are colored is rather trivial: this is because of extended delocalization involving amino groups, the heterocyclic core and phenyl rings. The extension of the frontier set to HOMO-1 and LUMO+1, which might be expected to mix in the first transition state, changes nothing, as both are of the same nature and have similar degrees of delocalization.

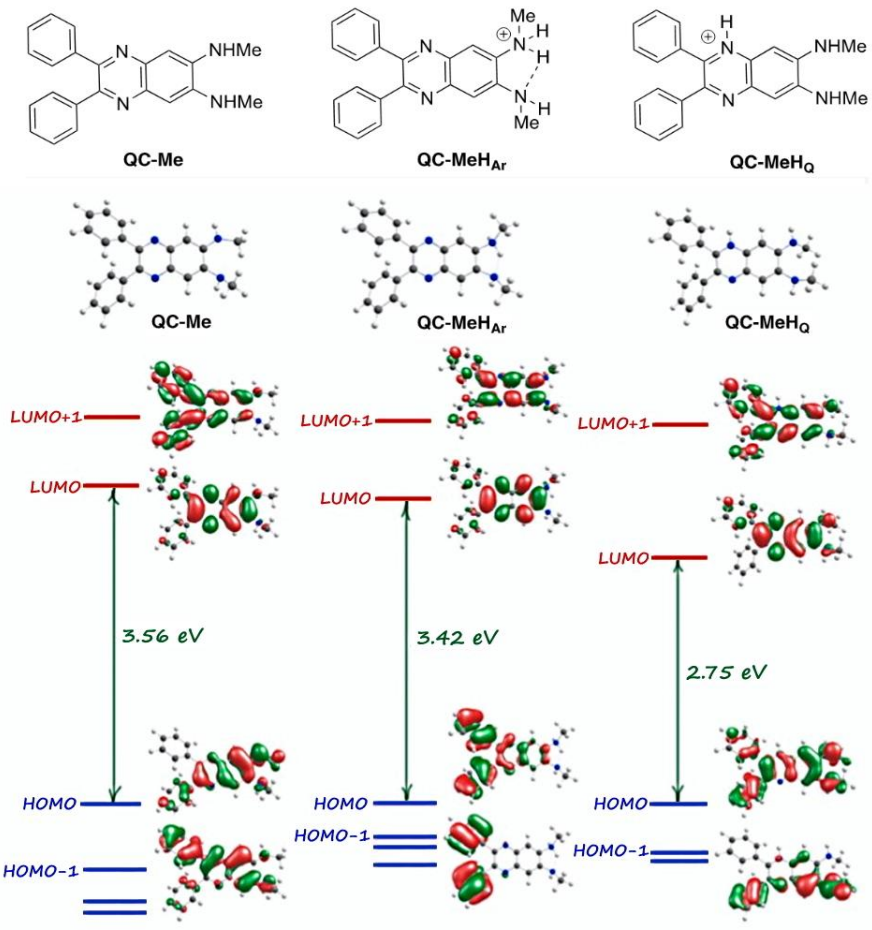

Figure 4. The isodensity plot of HOMO and LUMO orbitals for chromophores **QC-Me**, **QC-MeH$_{Ar}$** and **QC-MeH$_{Q}$** obtained from DFT calculations. The frontier orbitals are shown at the same scale and formally aligned at the respective HOMO levels.

Though the overall nature of transitions is similar in both the parent molecule **QC-Me** and two monoprotonated forms **QC-MeH$_{Ar}$** and **QC-MeH$_{Q}$**, the computations indeed help to reveal an essential difference between the latter. Protonation of the amino group (species **QC-MeH$_{Ar}$**) has surprisingly little effect on the electronic structure. Potentially, it can be readily understood as the second amino group remaining intact and continuing its role as a

donor substituent, and thus, the conjugation path remains almost undisturbed. The most important consequence is the conservation of the magnitude of the HOMO–LUMO gap in comparison with the unprotonated parent system **QC-Me**.

Protonation at the heterocyclic nitrogen has a much more pronounced influence, though the overall nature of the orbitals remains the same; thus, the lowest transition remains of the π–π* type. However, the HOMO–LUMO gap is much narrower. In the figure, we have artificially aligned all three systems using HOMO levels as a reference. In reality, the protonation leads to the stabilization of all levels of interest. The extent of stabilization is roughly dependent on the contribution of the protonated nitrogen AO to a given orbital. The protonation leads to an apparent increase in the effective atomic electronegativity, which, in turn, would lower the energy of any orbital to which this atom contributes its AO, and the higher is the contribution, the lower is the orbital. Figure 4, showing the frontier orbitals of interest, clearly reveals that in the compound **QC-MeH$_{Ar}$** protonated at the amino group, both frontier orbitals have a quite low contribution of ammonium nitrogen AO; therefore, the HOMO–LUMO gap remains unaffected. On the other hand, in the molecule **QC-MeH$_{Q}$** protonated at the heterocyclic nitrogen, both frontier orbital involves the protonated atom, and the contribution is markedly higher for LUMO, which is therefore lowered more strongly, resulting in narrowing the HOMO–LUMO gap. In terms of common resonance theory, the effect of ring protonation can be understood as improving the conjugation path by increasing the electron demand of the acceptor terminus.

Thus, we see that protonation at the amino group cannot explain the large red shift in both the absorption and emission spectra observed at higher acidity. Therefore, we conclude that the basicity of the ring nitrogens in these systems is higher than that of the aromatic amino group, and thus, this effect actually does follow the trend known in aminopyridine and aminoquinoline series. The basicity, however, is still rather meager, making the diaminoquinoxaline system a great choice for developing a pH indicator for a wide range of acidic pH values, including the high-acidity region.

To prove the structure of the protonated species, the titration of **QC1** in D_2O (1 mM solution) was also followed by ^{1}H NMR spectroscopy (Figure S7). First, the spectrum was recorded at pH 1, and all proton signals were unambiguously attributed based on their chemical shifts and coupling patterns (Figure S7). When pH was increased by adding a solution of NaOD in D_2O, significant upfield proton shifts were observed in the aromatic region at the pH range from 1 to 5 despite the compound's absence of protons located in the vicinal position to the nitrogen atoms of quinoxaline ring. Moreover, an upfield shift of methylene protons that are adjacent to external aromatic amino groups (δ_H 3.55–3.65) was observed, probably due to the significant contribution of two resonance forms in the structure of triprotonated species **B** (Scheme 2). Notably, similar changes in the position of methylene protons could be expected if an external aromatic nitrogen atom is protonated, affording tautomer **A**. Thus, these NMR data are in good agreement with the protonation scheme proposed based on UV–vis absorption and fluorescence data and DFT calculations (Scheme 2) but do not give additional information on the tautomeric structure of the triprotonated species. The spectra of **QC1** in basic solutions were broadened, probably due to the lower solubility of non-protonated **QC1** as compared to the diprotonated and triprotonated species, which are observed above pH 8.

The changes in absorption intensity at 480 nm and emission intensity based on ratiometric measurements (the pair I_{530} and I_{580} was used) with pH are shown in Figure 5. Using these S-type curves (Figure S8), quantitative measurements are possible in a rather large pH region. The addition of 10 equivalents of metal cations (K^+, Na^+, Mg^{2+}, Ba^{2+}, Ca^{2+}, Zn^{2+}, Co^{2+}, Cd^{2+}, Pb^{2+}, Ag^+, Ni^{2+}, Cu^{2+} and Al^{3+}) to an aqueous solution of **QC1** does not induce any changes in the absorption and emission of light (Figure S9). Only 10 equivalents of mercury(II) cations lead to the appearance of a shoulder at 480 nm in the UV–vis spectrum and causes a 10 nm bathochromic shift of the emission band (Figure S10). These changes probably result from the hydrolysis of mercury(II) salts in aqueous media

because the pH of the studied aqueous solution is decreased to 3.4 after the addition of 10 equivalents of Hg^{2+} perchlorate, and the electronic absorption and emission spectra of the solution thus obtained are almost identical to those of **QC1** at pH 3.4 (Figure S10).

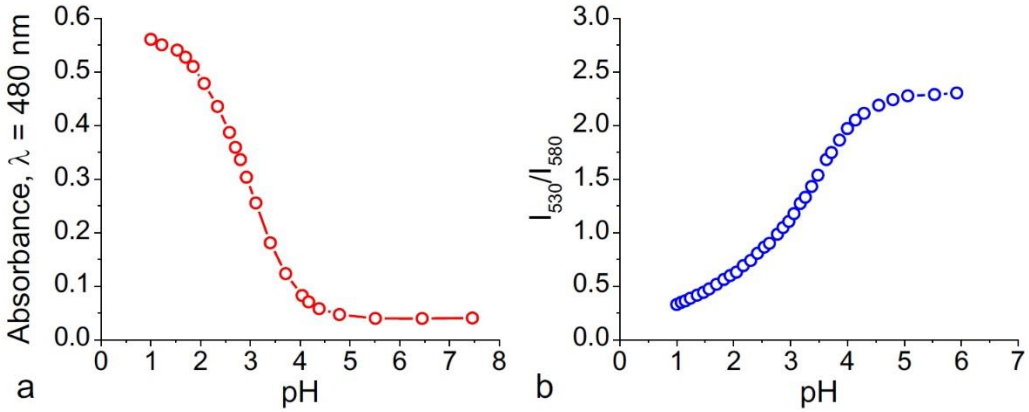

Figure 5. Changes in (**a**) absorption intensity (480 nm) and (**b**) emission intensity based on ratiometric measurements (the pair I_{530} and I_{580} was used) in the pH range of 1–7.

pH measurements performed using water from the Moscow River, which could contain many organic and inorganic contaminants relevant to real-life samples, confirmed that the **QC1** chemosensor is suitable for environmental monitoring. The halochromism of **QC1** in pure water and in this medium was completely identical, as shown in Figure S11.

Thus, aminoquinoxaline **QC1** can be used as a dual-responsive (spectrophotometric and fluorescent) indicator for monitoring pH of aqueous samples in strong acidic media (1–5). This indicator gives optical responses in the visible region and can be used for semi-quantitative naked-eye pH measurements. The protonation of primary amine groups remotes from the signaling group is observed in basic conditions, affording a diprotonated species that is highly soluble and exhibits halochromism under acidic conditions. It is noteworthy that functional chromophores showing shifts in both absorption and emission spectra upon an external stimulus (a proton in our case) are of great interest for sensor applications [29].

4. Conclusions

Quinoxalines have already been investigated as pH indicators, but only for pH monitoring in organic solvents or mixed organic solvent/water media due to their low solubility in aqueous media. In this work, we report the first water-soluble quinoxaline derivative for pH measurements in acidic (pH < 5) aqueous media in the absence of organic co-solvents.

We synthesized quinoxaline derivative **QC1** bearing (3-aminopropyl)amino residues at positions 6 and 7 of the heteroaromatic system using the Buchwald–Hartwig amination reaction as a key step. When this compound is dissolved in water, the spontaneous protonation of the primary amino group at pH lower than 8 is observed, leading to the formation of the water-soluble species displaying halochromism.

The water-soluble dual-responsive (absorbance and fluorescence) pH indicator **QC1** allows for efficient pH monitoring in acidic solutions (pH 1–5). This chromophore, displaying shifts in both absorption and emission spectra, can be used for quantitative pH measurements using appropriate instrumentation or semi-quantitative pH monitoring by the human eye. Common metal cations do not interfere, which is important for the analysis of real-world samples, which are commonly contaminated by environmentally relevant cations. We believe that such easily synthesized 6,7-diaminoquinoxalines, in which the structure of linear polyamine chains can be tuned and adapted to the analyte properties, could emerge as a powerful family of chemosensors with the biocompatible quinoxaline signaling group in the search for new compounds with stimulus-controlled optical properties.

Supplementary Materials: The following supporting information can be downloaded at: https://www.mdpi.com/article/10.3390/chemosensors10080342/s1. Figure S1: Normalized [0; 1] UV–vis absorption (a) and fluorescence (b) spectra of **QC1** in chloroform solution, [**QC1**] = 0.1 mM, λ_{ex} = 420 nm; Figure S2: UV–vis absorption (a) and fluorescence (b) spectra of **QC1** in an aqueous solution at pH 11.0 (*1*), 8.0 (*2*), 4.5 (*3*) and 1.0 (*4*). (a) [**QC1**] = 0.112 mM; (b) [**QC1**] = 0.015 mM, λ_{ex} = 420 nm; Figure S3: Dependence of the absorbance intensity on the **QC1** concentration in aqueous solutions at pH: 11.0 (a), 8.0 (b), 4.5 (c) and 1.0 (d); Table S1: Photophysical data for aminoquinoxaline **QC1** in aqueous solutions; Figure S4: Calculated with the HypSpec program: UV–vis absorption (a) and fluorescence (b) spectra of **QC1** (L), $[LH_2]^{2+}$ and $[LH_3]^{3+}$ in an aqueous solution; Figure S5: Distribution diagram of the protonated species of **QC1** (L) calculated with the HypSpec program based on UV–vis absorption (a) and fluorescence (b) spectra; Figure S6: pH-induced variation in the absorbance intensity corresponding to the absorption maxima 280 (a), 420 (b) and 480 nm (c) and fluorescence maxima 530 (d), 580 nm (e); Figure S7: ^{1}H NMR (400 MHz) spectra of **QC1** in D_2O at different pH values; Figure S8: Changes in (a) absorbance and (b) fluorescence intensity at 480 and 580 nm, respectively, and (c) the emission intensity based on the ratiometric ratio I_{530}/I_{580}: (*1*)—experimental data; (*2*)—fitting curve calculated according to the Boltzmann equation; Figure S9: UV–vis absorption (a) and fluorescence (b) spectra of **QC1** in aqueous solutions upon addition of 10 equiv. of metal perchlorates: K^+, Na^+, Mg^{2+}, Ba^{2+}, Ca^{2+}, Zn^{2+}, Co^{2+}, Cd^{2+}, Pb^{2+}, Ag^+, Ni^{2+}, Cu^{2+} and Al^{3+}, [**QC1**] = 0.1 mM, λ_{ex} = 420 nm; Figure S10: UV–vis absorption (a) and fluorescence (b) spectra of aqueous solution **QC1** upon addition of (*1*) 1 equiv. (*2*) and 10 equiv. (*3*) of $Hg(ClO_4)_2$ (pH 3.4) in aqueous solution at pH 3.4 (*4*), [**QC1**] = 0.2 mM, λ_{ex} = 420 nm; Figure S11: UV–vis absorption (a,b) and normalized [0; 1] fluorescence (c,d) spectra of aqueous solution of **QC1**: deionized water (a) and Moscow River (b) at different pH values, [**QC1**] = 0.319 mM, λ_{ex} = 420 nm.

Author Contributions: Conceptualization, A.B.-L.; methodology and investigation, E.V.E.; DFT calculations, A.V.C.; writing—original draft preparation, E.V.E. and A.V.C.; writing—review and editing, A.B.-L. and A.V.C.; visualization, E.V.E.; project administration, E.V.E. and A.B.-L.; funding acquisition, E.V.E. and A.B.-L. All authors have read and agreed to the published version of the manuscript.

Funding: This work was supported by Russian Foundation for Basic Research and Moscow City Government according to project №. 21-33-70003. Financial support from the CNRS, the Conseil Régional de Bourgogne (PARI IME SMT8 and PARI II CDEA programs) and the European Regional Development Fund (FEDER) is also acknowledged. E.V.E. is grateful to the French government and French embassy in Russia for the SSTE-2016 grant. This work was carried out in the frame of the International Associated French–Russian Laboratory of Macrocycle Systems and Related Materials (LIA LAMREM) of CNRS and RAS.

Institutional Review Board Statement: Not applicable.

Informed Consent Statement: Not applicable.

Data Availability Statement: Not applicable.

Acknowledgments: Penouilh Marie-José is warmly acknowledged for technical support.

Conflicts of Interest: The authors declare no conflict of interest.

References

1. Pereira, J.A.; Pessoa, A.M.; Cordeiro, M.N.D.S.; Fernandes, R.; Prudêncio, C.; Noronha, J.P.; Vieira, M. Quinoxaline, its derivatives and applications: A state of the art review. *Eur. J. Med. Chem.* **2015**, *97*, 664–672. [CrossRef]
2. Soleymani, M.; Chegeni, M. The chemistry and applications of the quinoxaline compounds. *Curr. Org. Chem.* **2019**, *23*, 1789–1827. [CrossRef]
3. Saranya, J.; Lavanya, K.; Kiranmai, M.H.; Subbiah, R.; Zarrouk, A.; Chitra, S. Quinoxaline derivatives as anticorrosion additives for metals. *Corros. Rev.* **2021**, *39*, 79–92. [CrossRef]
4. Chauhan, D.S.; Singh, P.; Quraishi, M.A. Quinoxaline derivatives as efficient corrosion inhibitors: Current status, challenges and future perspectives. *J. Mol. Liq.* **2020**, *320 Part A*, 114387. [CrossRef]
5. Montana, M.; Mathias, F.; Terme, T.; Vanelle, P. Antitumoral activity of quinoxaline derivatives: A systematic review. *Eur. J. Med. Chem.* **2019**, *163*, 136–147. [CrossRef]
6. Montana, M.; Montero, V.; Khoumeri, O.; Vanelle, P. Quinoxaline derivatives as antiviral agents: A systematic review. *Molecules* **2020**, *25*, 2784. [CrossRef]

7. Petronijevic, J.; Jankovic, N.; Bugarcic, Z. Synthesis of quinoxaline-based compounds and their antitumor and antiviral potentials. *Mini-Rev. Org. Chem.* **2018**, *15*, 220–226. [CrossRef]
8. Ajani, O.O.; Nlebemuo, M.T.; Adekoya, J.A.; Ogunniran, K.O.; Siyanbola, T.O.; Ajanaku, C.O. Chemistry and pharmacological diversity of quinoxaline motifs as anticancer agents. *Acta Pharm.* **2019**, *69*, 177–196. [CrossRef]
9. Ledwon, P.; Motyka, R.; Ivaniuk, K.; Pidluzhna, A.; Martyniuk, N.; Stakhira, P.; Baryshnikov, G.; Minaev, B.F.; Ågren, H. The effect of molecular structure on the properties of quinoxaline-based molecules for OLED applications. *Dyes Pigm.* **2020**, *173*, 108008. [CrossRef]
10. Yuan, J.; Ouyang, J.; Cimrová, V.; Leclerc, M.; Najari, A.; Zou, Y. Development of quinoxaline based polymers for photovoltaic applications. *J. Mater. Chem. C* **2017**, *5*, 1858–1879. [CrossRef]
11. Ji, S.-C.; Jiang, S.; Zhao, T.; Meng, L.; Chen, X.-L.; Lu, C.-Z. Efficient yellow and red thermally activated delayed fluorescence materials based on a quinoxaline-derived electron-acceptor. *New J. Chem.* **2022**, *46*, 8991–8998. [CrossRef]
12. Achelle, S.; Baudequin, C.; Plé, N. Luminescent materials incorporating pyrazine or quinoxaline moieties. *Dyes Pigm.* **2013**, *98*, 575–600. [CrossRef]
13. Dey, S.K.; Al Kobaisi, M.; Bhosale, S.V. Functionalized quinoxaline for chromogenic and fluorogenic anion sensing. *ChemistryOpen* **2018**, *7*, 934. [CrossRef] [PubMed]
14. da Silva, L.C.; Machado, V.G.; Menezes, F.G. Quinoxaline-based chromogenic and fluorogenic chemosensors for the detection of metal cations. *Chem. Pap.* **2021**, *75*, 1775–1793. [CrossRef]
15. Wang, T.; Douglass, E.F.; Fitzgerald, K.J.; Spiegel, D.A. A "Turn-On" fluorescent sensor for methylglyoxal. *J. Am. Chem. Soc.* **2013**, *135*, 12429–12433. [CrossRef] [PubMed]
16. Jo, S.; Kim, D.; Son, S.-H.; Kim, Y.; Lee, T.S. Conjugated poly(fluorene-quinoxaline) for fluorescence imaging and chemical detection of nerve agents with its paper-based strip. *ACS Appl. Mater. Interfaces* **2014**, *6*, 1330–1336. [CrossRef]
17. Singla, P.; Kaur, P.; Singh, K. Discrimination in excimer emission quenching of pyrene by nitroaromatics. *Tetrahedron Lett.* **2015**, *56*, 2311–2314. [CrossRef]
18. Wang, L.; Cui, M.; Tang, H.; Cao, D. Fluorescent nanoaggregates of quinoxaline derivatives for highly efficient and selective sensing of trace picric acid. *Dyes Pigm.* **2018**, *155*, 107–113. [CrossRef]
19. Benzeid, H.; Mothes, E.; Essassi, E.M.; Faller, P.; Pratviel, G. A thienoquinoxaline and a styryl-quinoxaline as new fluorescent probes for amyloid-β fibrils. *C. R. Chim.* **2012**, *15*, 79–85. [CrossRef]
20. Zhu, B.; Zhang, T.; Jiang, Q.; Li, Y.; Fu, Y.; Dai, J.; Li, G.; Qi, Q.; Cheng, Y. Synthesis and evaluation of pyrazine and quinoxaline fluorophores for in vivo detection of cerebral tau tangles in Alzheimer's models. *Chem. Commun.* **2018**, *54*, 11558–11561. [CrossRef]
21. Cui, M.; Ono, M.; Kimura, H.; Liu, B.; Saji, H. Novel quinoxaline derivatives for in vivo imaging of β-amyloid plaques in the brain. *Bioorg. Med. Chem. Lett.* **2011**, *21*, 4193–4196. [CrossRef] [PubMed]
22. Wencel, D.; Abel, T.; McDonagh, C. Optical chemical pH sensors. *Anal. Chem.* **2014**, *86*, 15–29. [CrossRef] [PubMed]
23. Khan, M.I.; Mukherjee, K.; Shoukat, R.; Dong, H. A review on pH sensitive materials for sensors and detection methods. *Microsyst. Technol.* **2017**, *23*, 4391–4404. [CrossRef]
24. Steinegger, A.; Wolfbeis, O.S.; Borisov, S.M. Optical Sensing and Imaging of pH values: Spectroscopies, materials, and applications. *Chem. Rev.* **2020**, *120*, 12357–12489. [CrossRef] [PubMed]
25. Isoda, K. Acid-responsive *N*-heteroacene-based material showing multi-emission colors. *ChemistryOpen* **2017**, *6*, 242–246. [CrossRef] [PubMed]
26. Black, H.T.; Pelse, I.; Wolfe, R.M.W.; Reynolds, J.R. Halochromism and protonation-induced assembly of a benzo[*g*]indolo[2,3-*b*]quinoxaline derivative. *Chem. Commun.* **2016**, *52*, 12877–12880. [CrossRef]
27. Aggarwal, K.; Khurana, J.M. Indeno–furan based colorimetric and on–off fluorescent pH sensors. *J. Photochem. Photobiol. A* **2015**, *307*, 23–29. [CrossRef]
28. Bag, R.; Sikdar, Y.; Sahu, S.; Maiti, D.K.; Frontera, A.; Bauzá, A.; Drew, M.G.B.; Goswami, S. A versatile quinoxaline derivative serves as a colorimetric sensor for strongly acidic pH. *Dalton Trans.* **2018**, *47*, 17077–17085. [CrossRef]
29. Mazumdar, P.; Maity, S.; Shyamal, M.; Das, D.; Sahoo, G.P.; Misra, A. Proton triggered emission and selective sensing of picric acid by the fluorescent aggregates of 6,7-dimethyl-2,3-bis-(2-pyridyl)-quinoxaline. *Phys. Chem. Chem. Phys.* **2016**, *18*, 7055–7067. [CrossRef]
30. Duffy, K.J.; Haltiwanger, R.C.; Freyer, A.J.; Li, F.; Luengo, J.I.; Cheng, H.-Y. Pyrido[1,2-*a*]quinoxalines: Synthesis, crystal structure determination and pH-dependent fluorescence. *J. Chem. Soc. Perkin Trans. 2* **2002**, 181–185. [CrossRef]
31. Gupta, S.; Milton, M.D. Design and synthesis of novel V-shaped AIEE active quinoxalines for acidochromic applications. *Dyes Pigm.* **2019**, *165*, 474–487. [CrossRef]
32. Moshkina, T.N.; Nosova, E.V.; Lipunova, G.N.; Valova, M.S.; Charushin, V.N. New 2,3-bis(5-arylthiophen-2-yl)quinoxaline derivatives: Synthesis and photophysical properties. *Asian J. Org. Chem.* **2018**, *7*, 1080–1084. [CrossRef]
33. Singh, P.; Baheti, A.; Thomas, K.R.J. Synthesis and optical properties of acidochromic amine-substituted benzo[*a*]phenazines. *J. Org. Chem.* **2011**, *76*, 6134–6145. [CrossRef] [PubMed]
34. Wang, M.; Wang, S.; Song, X.; Liang, Z.; Su, X. Photo-responsive oxidase mimic of conjugated microporous polymer for constructing a pH-sensitive fluorescent sensor for bio-enzyme sensing. *Sens. Actuators B* **2020**, *316*, 128157. [CrossRef]

35. Park, J.S.; Tran, T.T.; Kim, J.; Sessler, J.L. Electrochemical amphotericity and NIR absorption induced *via* the step-wise protonation of fused quinoxaline-tetrathiafulvalene-pyrroles. *Chem. Commun.* **2018**, *54*, 4553–4556. [CrossRef]
36. More, Y.W.; Padghan, S.D.; Bhosale, R.S.; Pawar, R.P.; Puyad, A.L.; Bhosale, S.V.; Bhosale, S.V. Proton triggered colorimetric and fluorescence response of a novel quinoxaline compromising a donor-acceptor system. *Sensors* **2018**, *18*, 3433. [CrossRef]
37. Safavi, A.; Abdollahi, H. Optical sensor for high pH values. *Anal. Chim. Acta* **1998**, *367*, 167–173. [CrossRef]
38. Tian, M.; Peng, X.; Fan, J.; Wang, J.; Sun, S. A fluorescent sensor for pH based on rhodamine fluorophore. *Dyes Pigm.* **2012**, *95*, 112–115. [CrossRef]
39. Yang, M.; Song, Y.; Zhang, M.; Lin, S.; Hao, Z.; Liang, Y.; Zhang, D.; Chen, P.R. Converting a solvatochromic fluorophore into a protein-based pH indicator for extreme acidity. *Angew. Chem. Int. Ed.* **2012**, *51*, 7674–7679. [CrossRef]
40. Li, H.; Guan, H.; Duan, X.; Hu, J.; Wang, G.; Wang, Q. An acid catalyzed reversible ring-opening/ring-closure reaction involving a cyano-rhodamine spirolactam. *Org. Biomol. Chem.* **2013**, *11*, 1805–1809. [CrossRef]
41. Xu, Y.; Jiang, Z.; Xiao, Y.; Bi, F.-Z.; Miao, J.-Y.; Zhao, B.-X. A new fluorescent pH probe for extremely acidic conditions. *Anal. Chim. Acta* **2014**, *820*, 146–151. [CrossRef] [PubMed]
42. Galloway, J.N. Acidification of the world: Natural and anthropogenic. *Water Air Soil Pollut.* **2001**, *130*, 17–124. [CrossRef]
43. Falkenberg, L.J.; Bellerby, R.G.J.; Connell, S.D.; Fleming, L.E.; Maycock, B.; Russell, B.D.; Sullivan, F.J.; Dupont, S. Ocean acidification and human health. *Int. J. Environ. Health Res.* **2020**, *17*, 4563. [CrossRef] [PubMed]
44. Petersen, M.H.; Gevorgyan, S.A.; Krebs, F.C. Thermocleavable low band gap polymers and solar cells therefrom with remarkable stability toward oxygen. *Macromolecules* **2008**, *41*, 8986–18994. [CrossRef]
45. Magde, D.; Wong, R.; Seybold, P.G. Fluorescence quantum yields and their relation to lifetimes of rhodamine 6G and fluorescein in nine solvents: Improved absolute standards for quantum yields. *Photochem. Photobiol.* **2002**, *75*, 327–1334. [CrossRef]
46. Gans, P.; Sabatini, A.; Vacca, A. Investigation of equilibria in solution. Determination of equilibrium constants with the HYPERQUAD suite of programs. *Talanta* **1996**, *43*, 1739–11753. [CrossRef]
47. Granovsky, A.A. Firefly Version 8. Available online: http://classic.chem.msu.su/gran/firefly/index.html (accessed on 20 June 2022).
48. Dolg, M.; Stoll, H.; Preuss, H.; Pitzer, R.M. Relativistic and correlation effects for element 105 (hahnium, Ha): A comparative study of M and MO (M = Nb, Ta, Ha) using energy-adjusted ab initio pseudopotentials. *J. Phys. Chem.* **1993**, *97*, 5852–5859. [CrossRef]
49. Lee, H.-Y.; Nepali, K.; Huang, F.-I.; Chang, C.-Y.; Lai, M.-J.; Li, Y.-H.; Huang, H.-L.; Yang, C.-R.; Liou, J.-P. (*N*-Hydroxycarbonylbenzylamino)quinolines as selective histone deacetylase 6 inhibitors suppress growth of multiple myeloma in vitro and in vivo. *J. Med. Chem.* **2018**, *61*, 905–1917. [CrossRef]
50. Yu, L.; Wu, Z.; Zhong, C.; Xie, G.; Wu, K.; Ma, D.; Yang, C. Tuning the emission from local excited-state to charge-transfer state transition in quinoxaline-based butterfly-shaped molecules: Efficient orange OLEDs based on thermally activated delayed fluorescence emitter. *Dyes Pigm.* **2017**, *141*, 325–1332. [CrossRef]
51. Li, S.-R.; Lee, C.-P.; Liao, C.-W.; Su, W.-L.; Li, C.-T.; Ho, K.-C.; Sun, S.-S. Structural engineering of dipolar organic dyes with an electron-deficient diphenylquinoxaline moiety for efficient dye-sensitized solar cells. *Tetrahedron* **2014**, *70*, 6276–16284. [CrossRef]
52. Lee, P.-I.; Hsu, S.L.-C.; Lin, P. White-light-emitting diodes from single polymer systems based on polyfluorene copolymers with quinoxaline derivatives. *Macromolecules* **2010**, *43*, 8051–18057. [CrossRef]
53. Witulski, B. Palladium-catalyzed synthesis of *N*-aryl- and *N*-heteroaryl-aza-crown ethers via cross-coupling reactions of aryl- and heteroaryl bromides with aza-crown ethers. *Synlett* **1999**, *1999*, 1223–11226. [CrossRef]
54. Ranyuk, E.; Douaihy, C.M.; Bessmertnykh, A.; Denat, F.; Averin, A.; Beletskaya, I.; Guilard, R. Diaminoanthraquinone-linked polyazamacrocycles: Efficient and simple colorimetric sensor for lead ion in aqueous solution. *Org. Lett.* **2009**, *11*, 987–990. [CrossRef] [PubMed]
55. Ermakova, E.; Michalak, J.; Meyer, M.; Arslanov, V.; Tsivadze, A.; Guilard, R.; Bessmertnykh-Lemeune, A. Colorimetric Hg^{2+} sensing in water: From molecules toward low-cost solid devices. *Org. Lett.* **2013**, *15*, 662–665. [CrossRef]
56. Ranyuk, E.; Ermakova, E.V.; Bovigny, L.; Meyer, M.; Bessmertnykh-Lemeune, A.; Guilard, R.; Rousselin, Y.; Tsivadze, A.Y.; Arslanov, V.V. Towards sensory Langmuir monolayers consisting of macrocyclic pentaaminoanthraquinone. *New J. Chem.* **2014**, *38*, 317–329. [CrossRef]
57. Arslanov, V.; Ermakova, E.; Michalak, J.; Bessmertnykh-Lemeune, A.; Meyer, M.; Raitman, O.; Vysotskij, V.; Guilard, R.; Tsivadze, A. Design and evaluation of sensory systems based on amphiphilic anthraquinones molecular receptors. *Colloids Surf. A* **2015**, *483*, 193–203. [CrossRef]
58. Ermakova, E.; Raitman, O.; Shokurov, A.; Kalinina, M.; Selector, S.; Tsivadze, A.; Arslanov, V.; Meyer, M.; Bessmertnykh-Lemeune, A.; Guilard, R. A metal-responsive interdigitated bilayer for selective quantification of mercury(II) traces by surface plasmon resonance. *Analyst* **2016**, *141*, 1912–1917. [CrossRef]
59. Abel, A.S.; Averin, A.D.; Cheprakov, A.V.; Roznyatovsky, V.A.; Denat, F.; Bessmertnykh-Lemeune, A.; Beletskaya, I.P. 6-Polyamino-substituted quinolines: Synthesis and multiple metal (Cu^{II}, Hg^{II} and Zn^{II}) monitoring in aqueous media. *Org. Biomol. Chem.* **2019**, *17*, 4243–4260. [CrossRef] [PubMed]
60. Beletskaya, I.P.; Bessmertnykh, A.G.; Guilard, R. Palladium-catalyzed synthesis of aryl-substituted polyamine compounds from aryl halides. *Tetrahedron Lett.* **1997**, *38*, 2287–2290. [CrossRef]
61. Beletskaya, I.P.; Bessmertnykh, A.G.; Averin, A.D.; Denat, F.; Guilard, R. Palladium-catalyzed arylation of linear and cyclic polyamines. *Eur. J. Org. Chem.* **2005**, *2005*, 261–280. [CrossRef]

62. Ruiz-Castillo, P.; Buchwald, S.L. Applications of palladium-catalyzed C–N cross-coupling reactions. *Chem. Rev.* **2016**, *116*, 12564–12649. [CrossRef] [PubMed]
63. Nosova, E.V.; Moshkina, T.N.; Lipunova, G.N.; Kopchuk, D.S.; Slepukhin, P.A.; Baklanova, I.V.; Charushin, V.N. Synthesis and photophysical studies of 2-(thiophen-2-yl)-4-(morpholin-4-yl)quinazoline derivatives. *Eur. J. Org. Chem.* **2016**, *2016*, 2876–2881. [CrossRef]
64. Zhang, Z.; Dai, Z.; Jiang, X. Copper-catalyzed aerobic oxidative dicarbonylation of indoles toward solvatochromic fluorescent indole-substituted quinoxalines. *Asian J. Org. Chem.* **2015**, *4*, 1370–1374. [CrossRef]
65. Sawicki, E.; Chastain, B.; Bryant, H.; Carr, A. Ultraviolet-visible absorption spectra of quinoxaline derivatives. *J. Org. Chem.* **1957**, *22*, 625–629. [CrossRef]
66. Justin Thomas, K.R.; Lin, J.T.; Tao, Y.-T.; Chuen, C.-H. Quinoxalines incorporating triarylamines: Potential electroluminescent materials with tunable emission characteristics. *Chem. Mater.* **2002**, *14*, 2796–2802. [CrossRef]